ACCELERATION OF ELECTRONS IN A DIFFRACTION DOMINATED IFEL

P. Musumeci, S. Ya. Tochitsky, S. Boucher, A. Doyuran, R. J. England,
C. Joshi, C. Pellegrini, J. Ralph, J. B. Rosenzweig, C. Sung, G. Travish, R. Yoder
University of California at Los Angeles, CA 90095, USA
A. Varfolomeev, S. Tolmachev, A. Varfolomeev Jr., T. Yarovoi, RRCKI, Moscow, Russia

Abstract

We report on the observation of energy gain in excess of 20 MeV at the Inverse Free Electron Laser Accelerator experiment at the Neptune Laboratory at UCLA. A 14.5 MeV electron beam is injected in a 50 cm long undulator strongly tapered both in period and field amplitude. A CO_2 10.6 μm laser with power $>$ 300 GW is used as the IFEL driver. The Rayleigh range of the laser ($\sim$ 1.8 cm) is shorter than the undulator length so that the interaction is diffraction dominated. Few per cent of the injected particles are trapped in stable accelerating buckets and electrons with energies up to 35 MeV are detected on the magnetic spectrometer. Three dimensional simulations are in good agreement with the electron energy spectrums observed in the experiment and indicate that substantial energy exchange between laser and electron beam only occurs in the first 25-30 cm of the undulator. An energy gradient of $>$ 70 MeV is inferred. In the second section of the undulator higher harmonic IFEL interaction is observed.

INTRODUCTION

Inverse Free Electron Laser (IFEL) schemes to accelerate particles have been proposed as advanced accelerators for many years [1, 2]. Recent successful proof-of-principle IFEL experiments have shown that along with acceleration [3, 4] this scheme offers the possibility to manipulate and control the longitudinal phase space of the output beam at the laser wavelength. First among other laser accelerator schemes, the Inverse Free Electron Laser has in fact experimentally demonstrated microbunching [5], phase-dependent acceleration of electrons [6], phase locking and multi-stage acceleration [7] and control of final energy spread [8]. Up to now, though, only modest energy gains and gradients have been achieved in an IFEL accelerator mostly because of the relatively low peak laser power employed in the experiments carried out so far.

The Inverse Free Electron Laser experiment at the Neptune laboratory at UCLA accelerated electrons from 14.5 MeV up to more than 35 MeV utilizing a CO_2 laser beam with a peak power ($\sim$ 0.4 TW), one order of magnitude greater than any other previous IFEL experiment had used. To maintain the resonant condition with the accelerating electrons, the 50 cm long undulator is strongly tapered both in period and magnetic field amplitude. An important point of the Neptune IFEL configuration is that the Rayleigh range of the laser beam is much shorter than the undulator length and the Inverse Free Electron Laser interaction is diffraction dominated.

EXPERIMENTAL SETUP

In Table 1 we report the design parameters of the Inverse Free Electron Laser experiment at the Neptune Laboratory.

In Fig. 1 it is shown the experimental layout for the IFEL experiment. An electron beam of 300 pC at 14.5 MeV is delivered to the experimental region by the Neptune rf photoinjector [9]. Final focus quadrupoles with large aperture to avoid clipping of the copropagating laser beam were installed on the beamline and focused the electron beam to the nominal spot size of 120 μm rms in the middle of the undulator. A TW-class CO_2 laser system [10] is used to drive the IFEL. The high power laser beam is brought in vacuum through a NaCl lens that has both the function of producing the correct focusing geometry and serves as a vacuum window. The laser is made collinear to the e-beam utilizing a plane copper mirror with a hole. The beams are aligned on the probe in the midplane of the undulator with an accuracy of $<$ 100 μm and the angular misalignment is kept below 1 mrad using the screens located before and after the undulator. After the interaction region, the e-beam is energy analyzed by the magnetic spectrometer and the laser beam is sent to the streak camera for timing measurements.

The undulator for the IFEL experiment at the Neptune Laboratory was built at the Kurchatov Institute [11]. It is a unique magnet because of the very strong variation of the undulator parameters (wiggling period and magnetic field amplitude) along the axis, carefully tailored to maintain the resonance condition of the IFEL interaction between the CO_2 photons and the quickly accelerating electrons. The undulator parameters are reported in Table 2.

Synchronization between electrons and photons is the

Electron beam	
energy	14.5 MeV
charge	0.3 nC
emittance	5 mm-mrad
pulse length (rms)	3 ps
CO_2 laser	
Power	400 GW
Wavelength	10.6 μ m
pulse length (rms)	100 ps
spot size	340 μ m

Table 1: Electron beam and CO_2 Laser parameters at the Neptune Laboratory

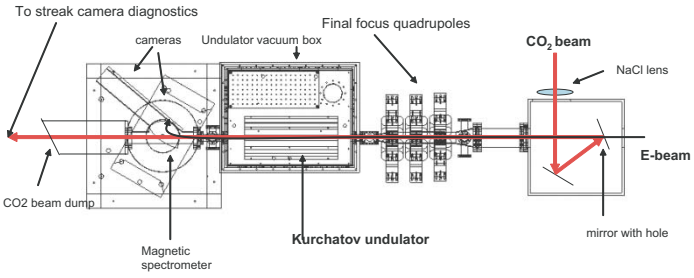

Figure 1: Layout of Neptune IFEL experiment

key for every laser accelerator with an externally injected electron beam and it is even more delicate in an IFEL experiment. In this kind of interaction in fact, there is no resonant medium (or cavity) where the accelerating electromagnetic wave is resonating and can live independently than the laser beam. The accelerator is virtually turned on only at the time the laser pulse goes through the undulator and the ponderomotive gradient that accelerates the electrons depends on the instantaneous power felt by the electrons.

At the Neptune laboratory, the electron pulse ($\sim$ 15 ps FWHM) and the longer CO_2 laser pulse ($\sim$ 240 ps FWHM) have been synchronized in the past with a cross-correlation method that was based on the e-beam controlled transmission of CO_2 through a Germanium sample. This technique [12] constituted the first step of the synchronization procedure also in the IFEL experiment. On the other hand, the cross-correlation measurement is conducted with the unamplified laser pulse propagating through the final triple passed, 2.5 m long multiatmosphere CO_2 amplifier with no inversion of population and has an intrinsic systematic error due to the different group velocity of the laser pulse within the inverted medium of the final amplifier in comparison with no-gain conditions. Moreover, fluctuations in laser power (gain in the final amplifier) $\pm$ 50 % cause fluctuations in the time of arrival of $\pm$ 50 ps. This jitter is intrinsic in the laser amplification system and could not be eliminated. In order to get very accurate information on the relative timing between the electrons and the amplified pulse on each shot, we set up a new streak camera based timing diagnostics.

In Fig. 2, it is shown a typical picture of the streak camera output. In the bottom left corner there is the reference green pulse from the photocathode drive laser that is representative of the electron timing. On the upper right side there is the streak of the CO_2 pulse. The delay (1170 ps) shown in Fig. 2 corresponds to the optimal timing and it was found maximizing the output IFEL energy as a function of delay. Utilizing the streak camera diagnostics, we were able to determine for each laser shot the pulse length (and so the peak power) of the CO_2 beam and which part of the laser pulse intensity profile the electron beam sampled with an accuracy of $\pm$ 10 ps.

The optical geometry used in the experiment to focus and control transversely the laser beam size is of particular importance. In the original design, a 2.56 m focal length NaCl lens focused the laser in the middle of the undulator to a spot size of 340 μm with a Rayleigh range of 3.5 cm to increase as much as possible the extent of the region where the beam is more intense. The resulting peak intensity is $2 \cdot 10^{14}$ W/cm^2 in the laser focus, about two orders of magnitude more than any previous IFEL experiment used [7, 8]. Dealing with this very high laser intensities on the other hand had some disadvantages.

Experimentally, in fact, we were limited by damage threshold on the last optical elements of the CO_2 transport line and we could not increase the f-number of the optical geometry as we planned. For our typical pulse lengths of 200 ps, we observed damage on the copper mirrors for fluences above 3J/cm^2 and on the single crystal NaCl optics for fluences above 2J/cm^2. In the end, we measured a spot size of 240 μm and Rayleigh range of 1.8 cm that, respect to the original design geometry, implied a stronger varia-

	initial	final
Undulator period	1.5 cm	5 cm
Magnetic field amplitude	0.16 T	0.65 T
K	0.2	2.8
Resonant energy	14.5 MeV	52 MeV

Table 2: RRCKI IFEL undulator parameters

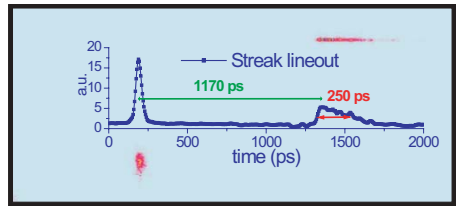

Figure 2: Streak camera picture of photocathode driver reference (lower-left corner) and CO2 pulse. The screen calibration gives a measurement of the laser pulse length and of the optimum delay between the reference and the CO2

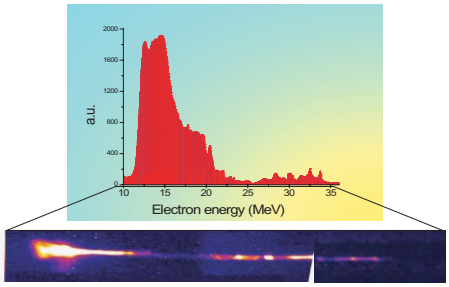

Figure 3: Single shot spectrum of the Inverse Free Electron Laser accelerator. More than 5 % of particles are accelerated to 35 MeV with 150 % energy gain

tion of the beam size along the interaction region, and with the same nominal focus position at the mid-point of the undulator, a larger and less intense beam at the entrance and exit of the undulator.

To trap and accelerate particles along the design resonant orbit, the ponderomotive IFEL gradient generated by the laser electric field has to match the designed tapering gradient. If this is not the case, no trapping or acceleration are possible. Because of the differences between nominal and measured Rayleigh range, it was found out necessary to move the laser focus upstream from the nominal position to increase the intensity at the undulator entrance above the trapping threshold and start the acceleration process early in the undulator. Of course that would also cause the particles to fall out of resonance soon after the mid point of the undulator because of lack of enough ponderomotive force to sustain the acceleration along the designed orbit. It was found that the optimum position of the laser focus for the power levels available, was 2 cm (one Rayleigh range) upstream of nominal focus position.

EXPERIMENTAL RESULTS AND SIMULATIONS

The electrons were detected by a phosphorous screen observed by CCD cameras. The screen was attached to the thin mylar window at the exit slit of the spectrometer. Different neutral density filters were applied to each cameras to get unsaturated images of the output slit. A postprocessing application that takes into account the different filters and scales the horizontal axis of the images with energy, reconstructed the single shot spectrum of the electron beam out of the IFEL accelerator for each laser shot. A typical image of a dispersed electron beam is presented in Fig. 3 along with a reconstructed spectrum.

The energy spectrum shows more than 5 % of particles trapped and accelerated up to 35 MeV with a 150 % energy gain. The measured power in the CO_2 pulse for this IFEL shot was 400 GW of power and the laser was focused upstream of the nominal position by 2 cm.

The code that was used to simulate the experiment at the design phase is a 4th-order Runge-Kutta integrator that solved the Lorentz equation for the particle motion in the combined fields of the undulator magnet and laser beam (TREDI[13]). The same code was used to understand the experimental results reproducing the experimental condition, and, once we put the correct laser intensity profile along the undulator, agree quite well with the experiment.

In Fig. 4 the simulated longitudinal phase-spaces at two different distances along the undulator are shown. The histograms on the left of the graphs are the projection of the phase-spaces on the energy axis. The simulation results allowed us to draw several conclusions.

First of all (Fig. 4a) that the IFEL acceleration mostly takes place in the first section of the undulator (first 25 cm). Few cm after the mid-point the laser intensity has decreased below the trapping threshold and the designed tapering is too strong for the particles too follow. That allows us to infer an accelerating gradient of > 70 MeV/m.

Secondly, Fig. 4b shows the structure of the high energy side of the spectrum observed in the experiment. This structure is particularly interesting because experimentally it was reproducible shot to shot, ruling out the possibility of micro-structures present in the e-beam or the laser beam. Instead, the structure is due to a different kind of IFEL interaction that takes place in the second section of the undulator.

We know that efficient energy exchange between the transverse EM wave and the particles wiggling in the undulator can only take place when the resonant condition is satisfied, and so the energy of the particles is such that in the electron's rest frame the wiggling induced by the undulator has the same frequency of the wiggling induced by the laser. On the other hand, it is known that particles of a fixed energy going through an undulator interact not only with the fundamental resonant frequency, but also with the radiation harmonics [14]. From another point of view, particles of different energy $\gamma_{r,n}$ can interact with the same laser frequency, because they see the EM wave as a higher harmonic of the fundamental frequency that they are resonant with. In other words, for a given laser and undulator,

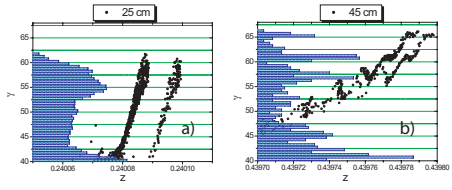

Figure 4: Simulations of IFEL longitudinal phase space at different points along the z axis. a) Longitudinal phase space at the undulator mid-point. The energy gain has already taken place in 25 cm. b) Energy modulation due to second harmonic interaction in the second section of the undulator. The structure in the simulated spectrum corresponds to the one in the measured spectrum

there are multiple resonant energies

$$\gamma_{r,n} = \sqrt{\frac{\lambda_w \cdot \left(1 + \frac{K^2}{2}\right)}{2\lambda \cdot n}} \quad (1)$$

In Fig. 5, we show the first three resonant energy curves for the Neptune IFEL undulator. In the experiment the particles fall out of the accelerating bucket from the resonant curve (red) because of the mismatched laser intensity distribution. At some point later in the undulator the particles energy is $1/\sqrt{2}$ times the resonant energy, at this point the electrons can exchange energy with the 10.6 μm photons mediated by the second harmonic IFEL interaction.

The equations for the Higher Harmonics IFEL interaction are the standard IFEL equation, with the coefficient JJ for the first harmonic interaction replaced by the appropriate $\mathtt{JJ}_n$ coupling coefficient [15].

$$\mathtt{JJ}_n = \sum_{m=-\infty}^{+\infty} J_m(\xi) \cdot (J_{2m+n+2}(\sigma) - J_{2m+n}(\sigma)) \quad (2)$$

with dependence on the undulator K factor hidden in $\xi = K^2/(4+2K^2)$, the usual Bessel function argument, and in $\sigma = K/(\gamma k_w w)$ where k_w is the undulator wave number and w is the laser spot size.

The parameter σ taking a closer look, is the ratio of the particles wiggling amplitude to the laser spot size, and it can be viewed as a quantitative measure of how three-dimensional the interaction is. We note that the even harmonics interaction should be suppressed as a consequence of the known fact that the on-axis spectrum of a planar undulator has only the odd harmonics. This is reflected by the behavior of the coupling coefficients for even harmonics (i.e. $\mathtt{JJ}_n \rightarrow 0$ when $\sigma \rightarrow 0$. for even n). In other words σ determines the strength of the IFEL coupling to the even harmonics [16].

In the Neptune experiment, the trajectory wiggling amplitude increases along the undulator and it becomes comparable to the laser beam size around the focus region. The σ parameter reaches relatively large values (~ 0.5) and the second harmonic IFEL coupling is not negligible. Moreover, in this region of the undulator the CO_2 laser is still very intense, so that a significant amount of energy can be transferred to the e-beam. The longitudinal modulation induced by HHIFEL interaction that appears in the simulated phase space is washed out after a short drift propagation, because of the large energy spread. On the other hand, the deep energy structure resulting from this kind of interaction remains imprinted on the experimental beam energy spectrum. The energy exchange is not as efficient for the third harmonic IFEL interaction that could take place at the end of the undulator. Here, regardless of the strength of the coupling constant, the laser field is just not intense enough to perturb significantly the electron energy spectrum.

The higher harmonic interaction is the origin of the energy modulation seen reproducibly in the output spectrum of the experiment.

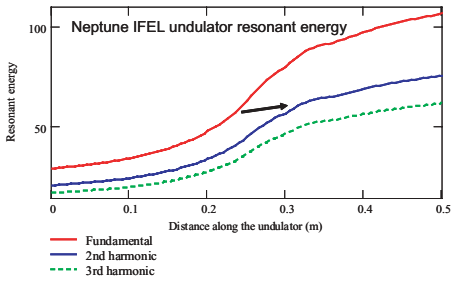

Figure 5: Neptune IFEL undulator different resonant energies.

CONCLUSION

We report on the observation of $>$ 20 MeV energy gain (150 %) at the Inverse Free Electron Laser experiment at the Neptune Laboratory. An energy gradient of $>$ 70 MeV/m is inferred. The fraction of self-trapped particles exceeded 5 % of the injected bunch. The acceleration gain reported is to date the highest obtained with an IFEL accelerator. Self-trapping of particles in a stable accelerating bucket from a not-prebunched initial distribution was demonstrated. The effects of the laser diffraction were analyzed in the design phase and studied experimentally. Finally, for the first time higher harmonic IFEL (HH-IFEL) interaction was observed in the second section of the undulator. The HH-IFEL adds a degree of freedom (the harmonic coupling number n) in the design of magnetic systems capable of coupling lasers and electron beams. This work is supported by U.S. Dept. of Energy grant DE-FG03-92ER40693

REFERENCES

[1] R.B. Palmer. *J. Applied Physics*, 43:3014, 1972.

[2] E. D. Courant, C. Pellegrini, and W. Zakowicz. *Phys. Rev. A*, 32:2813, 1985.

[3] I. Wernick and T. C. Marshall. *Phys. Rev. A*, 46:3566, 1992.

[4] A. Van Steenbergen et al. *Phys. Rev. Lett.*, 77:2690, 1996.

[5] Y. Liu et al. *Phys. Rev. Lett.*, 80:4418, 1998.

[6] R. B. Yoder, T. C. Marshall, and J. L. Hirshfield. *Phys. Rev. Lett.*, 86:1765, 2001.

[7] W. Kimura et al. *Phys. Rev. Lett.*, 86:4041, 2001.

[8] W. Kimura et al. *Phys. Rev. Lett.*, 92:054801, 2004.

[9] S. G. Anderson et al. *AIP Conf. Proc.*, 569:487, 2000.

[10] S. Ya. Tochitsky et al. *Opt. Lett.*, 24:1717, 1999.

[11] S. Tolmachev et al. these proceedings

[12] S. Ya. Tochitsky et al. *Phys. of Plasmas*, 11:2875, 2004.

[13] L. Giannessi, P. Musumeci, M. Quattromini *Nucl. Instr. Meth. A*, 436:443, 1999.

[14] Z. Huang and K. J. Kim. *Phys. Rev. E*, 62:7295, 2000.

[15] P. Musumeci et al. 2004. to be submitted for publication.

[16] M. J. Schmidt and C. J. Elliot *Phys. Rev. A*, 34:4843, 1986.